processes

MDPI

Article

Brownian Motion and Thermophoretic Effects in Mini Channels with Various Heights

Zainab Al Hajaj [1] and Mohamad Ziad Saghir [2,*]

[1] Department of Mechanical Engineering, Australian College of Kuwait, P.O. Box 1411, Safat 13015, Kuwait; z.hajaj@ack.edu.kw
[2] Department of Mechanical and Industrial Engineering, Ryerson University, Toronto, ON M5B 2K3, Canada
* Correspondence: zsaghir@ryerson.ca

Abstract: Flow-through mini channels have received tremendous interest from researchers over a long period. However, the study of flow between the channel and on top of the channel has received little to no attention. In the present paper, different parameters have been used to investigate this heat enhancement. The height of 10 mini channels has been varied, allowing the corresponding aspect ratio to vary from 3 to 6, 9, and 12. When the aspect ratio is 12, flow circulates through the mini channel only, and when the aspect ratio is less than 12, flow is distributed between the one circulating inside the channel and moving on top of the channel. Different flow rates are studied corresponding to a Reynolds number varying from 250 to 1250 if water is the working fluid. Brownian and thermophoresis effects are taken into consideration to investigate the nanoparticle sedimentation. Results revealed that the optimum configuration, if one needs to take into consideration the friction factor, is 12. If one ignores the pressure drops, then the optimum configuration is when the aspect ratio is equal to 6. This means that the flow interaction between the one circulating in the channel and above the channel plays a major effect in heat removal.

Keywords: Brownian motion; thermophoretic effect; two-phase flow; nanofluid; channels

check for updates

Citation: Al Hajaj, Z.; Saghir, M.Z. Brownian Motion and Thermophoretic Effects in Mini Channels with Various Heights. *Processes* **2021**, *9*, 1965. https://doi.org/10.3390/pr9111965

Academic Editors: Zhichun Liu and Chen Yang

Received: 27 September 2021
Accepted: 1 November 2021
Published: 3 November 2021

Publisher's Note: MDPI stays neutral with regard to jurisdictional claims in published maps and institutional affiliations.

Copyright: © 2021 by the authors. Licensee MDPI, Basel, Switzerland. This article is an open access article distributed under the terms and conditions of the Creative Commons Attribution (CC BY) license (https://creativecommons.org/licenses/by/4.0/).

1. Introduction

Heat improvement is an attractive topic in engineering which falls under heating and cooling. In some applications, cooling is required for machinery efficiency. Many researchers [1–17] have conducted experimental and numerical works by studying flow in the channel, flow in porous channels, and other shape channels like wavy channels. They used water and/or nanofluid as a working fluid. Different concentrations of nanoparticles were investigated experimentally and later numerically. Overall, heat enhancement by using nanofluid did not exceed 5%.

Other work with alumina conducted by Ho et al. [18] examined the results of including nanofluid in a mini-channel heat sink with microencapsulated phase change material. Again, they examined a large range of nanofluid concentrations from 0 to 8% wt. They noted that the largest concentration of nanoparticles resulted in the largest increase in the average heat transfer effectiveness of 1.4 and a figure of merit increase of 1.27. Another contribution by Ho et al. [19] examined the same concentration as their previous work of 0–8% wt of Al_2O_3 nanofluid in water but did not include the MEPCM in their testing apparatus. They did, however, reach the same increase in the heat transfer effectiveness and figure of merit as a result of the inclusion of the nanofluids, showing that the nanofluid has a significant impact on the thermal performance of the system. Another investigation into the performance of Al_2O_3 nanofluids in water was conducted by Hader and Al-Kouz [20]. In their work, they examined a photovoltaic system combined with a heat exchanger using fins and parallel plates. They examined a numerical model created in COMSOL to investigate the efficiency of the system. They observed that as the nanoparticle concentration was increased, the performance of the system would subsequently increase.

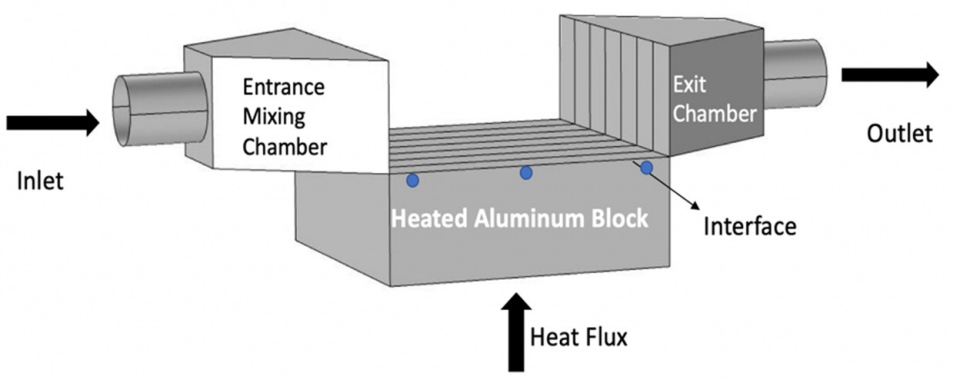
Brownian motion and thermophoresis effects have been studied in detail by many researchers [21–29]. Their studies covered a large range of engineering configurations with the ultimate goal of heat enhancement. Amongst them, Bondareva et al. [30] studied the natural convection of nanofluid water based in a partially open trapezoidal cavity under the influence of Brownian and Thermophoresis effects. The uniqueness of this article is an open-sided cavity. Results revealed that at high Rayleigh and Lewis numbers, a homogenization of nanoparticle distribution is evident. Sheremet et al. [31] investigated steady-state free convection in a right-angle triangle filled with a porous material. The fluid used was nanofluid, and numerically, the Buongiorno model was adapted. Results revealed that the average Nusselt number increases as a function of Rayleigh and Lewis numbers in the presence of Brownian and Thermophoresis effects. Moreover, Khan et al. [32] explored the three-dimensional rotating flow of a nanofluid in the presence of Brownian and thermophoresis motions. Results revealed that the increase in thermophoresis effects lead to a decrease in temperature, respectively.

In our present study, we investigate numerically the usefulness of using nanofluid in heat enhancement. We consider ten-rectangular mini channel configurations in the presence of Brownian motion and the thermophoresis effect. Nanoparticle distributions are examined for different nanofluid diameters and at various Reynolds numbers. The channel's height has been varied from a short channel to a full height channel. The channel is located inside a cavity; thus, interaction between flow through the channel and above channels will be discussed. In addition, we investigated two different nanoparticle diameters and compared the effectiveness of the size of the nanoparticle in heat enhancement in a mini channel with different heights. Additionally, the flow interaction between the one circulating above the channels and the one circulating in the channels will be investigated. Section 2 presents the problem description, the boundary conditions and mesh sensitivity. The formulation in the non-dimensional form is presented in Section 3. Section 4 presents the results and discussion, followed by the conclusion in Section 5.

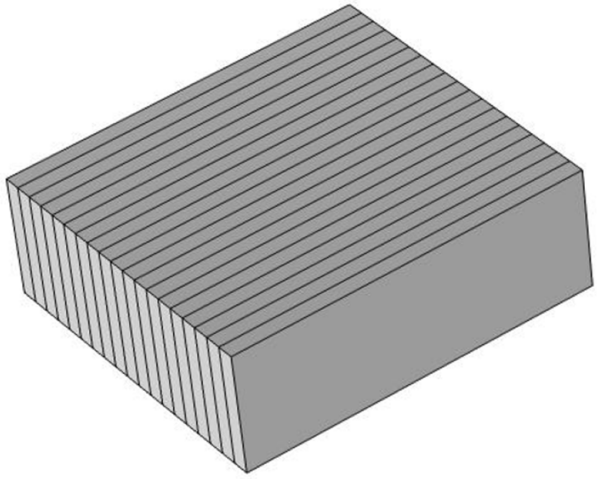
2. Problem Description and Boundary Conditions

This paper examines different fluid performances in ten mini channel configurations towards experimenting. Figure 1 presents the model under investigation. The numerical setup consists of an inlet pipe, a mixing chamber, a flow-through three channels, and finally an outlet through which the fluid exits from the opposite side. The bottom of the plate is in direct contact with an aluminum block heated with thermal resistance. Each channel has the dimensions: a width of 1.785 mm, height of 12.7 mm, and length of 37.5 mm. The insert is a square cavity that consists of ten channels with 37.5 mm in width and variable height. Four different aspect ratios (AR) for this insert will be investigated, which are AR = 3, 6, 9, and 12, corresponding to a channel height of 3.41 mm, 6.82 mm, 10.21 mm, and 12.7 mm, respectively. The aluminum block underneath the insert has the same dimensions of a 37.5 mm square side and 12.7 mm thickness. Aluminum is used in our modeling to match the prepared experimental setup. The fluid enters with a velocity u_{in} and a temperature T_{in}. The temperature is calculated numerically 1 mm below the so-called interface located at the center of the insert.

Figure 1a presents the model which we adopted in our analysis. As one may notice, the dots are the places where the fluid temperature is calculated. Figure 1b presents the insert which will fit in the setup shown in Figure 1a. A thermo-paste will be spread at the interface modeling as a thin thermal layer. The material for the channels is made of aluminum, similar to the other parts of the setup. The three-dimensional model is used because it is expected that the flow intensity in the middle channels will be different from the other channels. In our analysis, different flow rates will be applied corresponding to different Reynolds numbers.



(**a**) Model setup



(**b**) Channels insert

Figure 1. A geometrical model with a different insert. (**a**) Experimental setup. (**b**) Insert mini channels.

The pressure drop for the friction factor is measured at the entrance and exit of the mixing chamber. Thus, it is the pressure drop for the entire insert. Using the average velocity, we calculated the friction factor along the flow direction (Z-direction) for the entire setup. Constant heat flux is applied at the bottom of the setup of 50,000 W/m^2 and, in non-dimensional form, is equivalent to 1. Our working fluids are water and 1% vol Al_2O_3/water, with two different nanoparticle diameters of 31 nm and 100 nm. Table 1 presents the physical properties of these nanofluids for different nanoparticle sizes.

Table 1. Physical properties of the nanofluids [33].

Fluids	μ	ρ	Cp (J/kg/K)	k (W/m/K)
Water	0.001002	998.2	4182	0.598
1%vol Al_2O_3/Water (dp = 31 nm)	0.00107	1024.218	4061.89	0.6322
1%vol Al_2O_3/Water (dp = 100 nm)	0.00106	1024.218	4061.89	0.6196

3. Finite Element Analysis

Assuming a steady-state condition and laminar flow, the Navier–Stokes equations in the non-dimensional form are shown in Equation (1) to Equation (7). The formulation for the Brownian motion and thermophoretic effects are taken from [27]. The proposed formulations are as follows.

3.1. Fluid Flow Formulation

To make the governing equations of the physical model dimensionless, we define the following set of transformations.

$$X = \frac{x}{D},\ Y = \frac{y}{D},\ Z = \frac{z}{D},\ U = \frac{u}{u_{in}},\ V = \frac{v}{u_{in}},\ W = \frac{w}{u_{in}}, P = \frac{pD}{\mu_{nf} u_{in}},\ \tau = \frac{t u_{in}}{D},\ \theta = \frac{(T - T_{in})k_w}{q'' D} \quad (1)$$

The dimensionless parameters, such as Reynolds number (Re), Schmidt number (Sc), and Lewis number (Le), are defined by

$$Re = \frac{\rho u_{in} D}{\mu},\ Pr = \frac{\nu_{nf}}{\alpha_{nf}},\ Le = \frac{\alpha_{nf}}{D_m} \text{ and } Sc = \frac{\nu_{nf}}{D_m} \quad (2)$$

Here, u_{in} is the velocity at the inlet as shown in Figure 1. The subscript "nf" is for the nanofluid used in our calculation. The molecular diffusion is known here as D_m.

The full Navier–Stokes equations in the three-dimensional form are as follows.

X-direction:

$$Re\left[\frac{\partial U}{\partial \tau} + U\frac{\partial U}{\partial X} + V\frac{\partial U}{\partial Y} + W\frac{\partial U}{\partial Z}\right] = -\frac{\partial P}{\partial X} + \left[\frac{\partial^2 U}{\partial X^2} + \frac{\partial^2 U}{\partial Y^2} + \frac{\partial^2 U}{\partial Z^2}\right] \quad (3)$$

Y-direction:

$$Re\left[\frac{\partial V}{\partial \tau} + U\frac{\partial V}{\partial X} + V\frac{\partial V}{\partial Y} + W\frac{\partial V}{\partial Z}\right] = -\frac{\partial P}{\partial Y} + \left[\frac{\partial^2 V}{\partial X^2} + \frac{\partial^2 V}{\partial Y^2} + \frac{\partial^2 V}{\partial Z^2}\right] \quad (4)$$

Z-direction:

$$Re\left[\frac{\partial W}{\partial \tau} + U\frac{\partial W}{\partial X} + V\frac{\partial W}{\partial Y} + W\frac{\partial W}{\partial Z}\right] = -\frac{\partial P}{\partial Z} + \left[\frac{\partial^2 W}{\partial X^2} + \frac{\partial^2 W}{\partial Y^2} + \frac{\partial^2 W}{\partial Z^2}\right] \quad (5)$$

Here, U, V, and W are the velocities along the X, Y, and Z directions.

3.2. Heat Transfer Formulation

The energy equation for the fluid portion is the following:

$$RePr\left[\frac{\partial \theta}{\partial \tau} + U\frac{\partial \theta}{\partial X} + V\frac{\partial \theta}{\partial Y} + W\frac{\partial \theta}{\partial Z}\right] = \left[\frac{\partial^2 \theta}{\partial X^2} + \frac{\partial^2 \theta}{\partial Y^2} + \frac{\partial^2 \theta}{\partial Z^2}\right] + Q \quad (6)$$

where Q is the heat source and is equal to

$$Q = \frac{H}{Le}\left(\frac{\partial C}{\partial X}\frac{\partial \theta}{\partial X} + \frac{\partial C}{\partial Y}\frac{\partial \theta}{\partial Y} + \frac{\partial C}{\partial Z}\frac{\partial \theta}{\partial Z}\right) + \frac{H}{Le}\frac{Sor}{\overline{\theta}}\left(\left(\frac{\partial \theta}{\partial X}\right)^2 + \left(\frac{\partial \theta}{\partial Y}\right)^2 + \left(\frac{\partial \theta}{\partial Z}\right)^2\right)^2 \quad (7)$$

The term H is equal to the ratio of the heat capacity of the nanoparticles divided by the heat capacity of the nanofluid. Thus, H is equal to $\frac{(\rho Cp)_p}{(\rho Cp)_{nf}}$. The constant term Sor is the ratio of $\frac{D_T}{D_m}$.

The molecular diffusion D_m and the thermophoretic effect D_T are expressed as follows [34]:

$$D_m = \frac{k_B\, T_{average}}{3\pi \mu_b d_p} \quad (8)$$

Here, k_B is the Boltzmann constant and is equal to 1.38×10^{-23}, d_p is the nanoparticle diameter in meters, $T_{average}$ is the average temperature, and μ_b is the viscosity of the base fluid, which is water here. The thermophoretic diffusion coefficient or so-called thermal diffusion coefficient is

$$D_T = 0.26\frac{k_w}{2k_w + k_p}\left(\frac{\mu_w}{\rho_w}\right) \times \phi \quad (9)$$

Here, k_w is the conductivity of the base fluid, k_p is the conductivity of the nanoparticles, μ_w is the dynamic viscosity of the water, and ρ_w is the density of the water. The concentration of the nanoparticles is ϕ and is equal to 0.01.

3.3. Mass Transfer Formulation

The mass transfer equation in dimensionless form is

$$\mathrm{Re.Sc}\left[\frac{\partial C}{\partial \tau}+U\frac{\partial C}{\partial X}+V\frac{\partial C}{\partial Y}+W\frac{\partial C}{\partial Z}\right]=\left[\frac{\partial^2 C}{\partial X^2}+\frac{\partial^2 C}{\partial Y^2}+\frac{\partial^2 C}{\partial Z^2}\right]+\frac{H}{Le}\mathrm{Sor}\left(\frac{\partial^2 \theta}{\partial X^2}+\frac{\partial^2 \theta}{\partial Y^2}+\frac{\partial^2 \theta}{\partial Z^2}\right) \quad (10)$$

Finally, the temperature in the solid part of the model is studied by solving the heat conduction formulation. The local Nusselt number is known as the ratio of the convective heat coefficient multiplied by the characteristic length over the water conductivity (i.e., $\frac{hD}{k_w}$). The characteristic length D is set equal to 0.01897 m. Based on the non-dimensional adopted earlier, it becomes the inverse of the temperature. Thus,

$$Nu=\frac{1}{\theta}*\left(\frac{k_{nf}}{k_w}\right) \quad (11)$$

The friction factor is known as being the ratio of the pressure drop to the kinetic energy of the fluid. The friction factor in a non-dimensional form used in our analysis is

$$f=0.2529*\frac{\Delta P}{Re} \quad (12)$$

The performance evaluation criterion (PEC) shown in Equation (13) combines the heat effect and the flow effect. Thus,

$$PEC=\frac{Nu_{average}}{f^{\frac{1}{3}}} \quad (13)$$

The heat removed from the system is worth investigating independently from the flow behavior. Equation (14) represents the non-dimensional form. Thus,

$$Q=Re*Pr*\theta_{out} \quad (14)$$

The parameter explained in this section will be used in our investigation.

3.4. Mesh Sensitivity

The mesh sensitivity was conducted to make sure the optimum mesh is applied.

Table 2 presents a different type of mesh following the COMSOL approach, and Figure 2 shows the optimum mesh used in our analysis, which is mesh level fine. This decision was made after being able to measure the average Nusselt number and finding that the changes between normal and fine are less than 2.5%

Table 2. Mesh information for a different level of meshing [35].

Extremely coarse	14,136 elements
Extra coarse	28,166 elements
Coarser	48,642 elements
Coarse	121,820 elements
Normal	214,624 elements
Fine	527,094 elements
Finer	1,469,293 elements

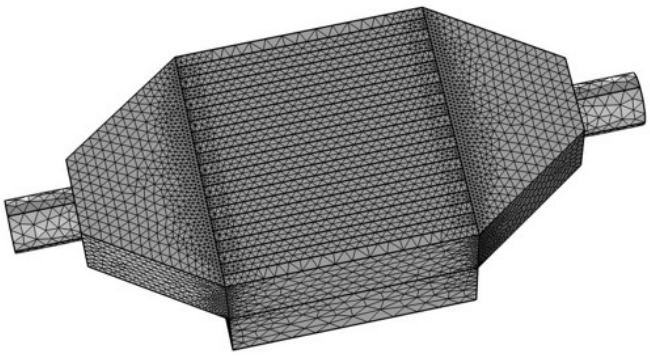


Figure 2. Finite element analysis [35].

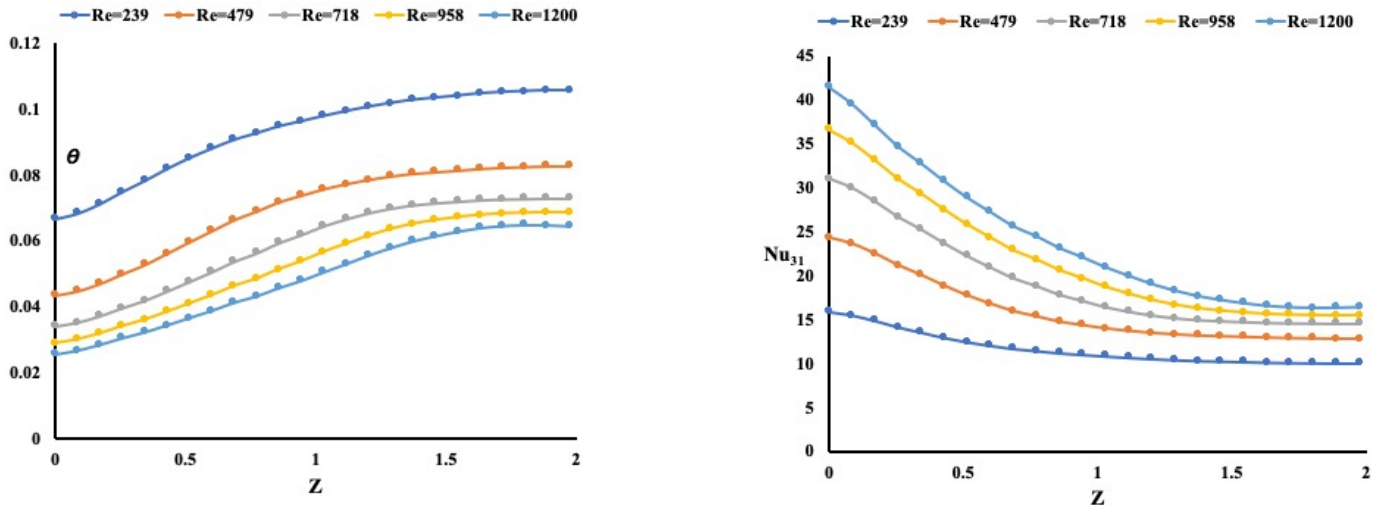
4. Results and Discussions

In the present study, we investigate the different parameters towards understanding better heat enhancement using multiple channels. The fluid flow rate represented by the Reynolds number (Re) used in our analysis has a value of 250, 500, 750, 1000, and 1250 if water is the circulating fluid. A different Reynolds number is used for the nanofluid case because by maintaining a constant flow rate, the viscosity of the nanofluid is different than water viscosity. In that case, 1% vol Al_2O_3/water with a nanoparticle diameter of 31 nm corresponds to a Reynolds number (Re_{31}) of 239, 479, 718, 958, and 1200, respectively. When the nanoparticle diameter changes to 100 nm, the corresponding Reynolds (Re_{100}) number becomes 242, 485, 727, 970, and 1210, respectively. Thus, depending on the fluid under investigation, the Reynolds number may vary accordingly, and the flow is in the laminar regime. A steady-state condition is applied, and the fluid is assumed to be a Newtonian fluid. Another variable that is also discussed is the aspect ratio. In the present case, for an aspect ratio equal to 12, this means that the channel has a full height, and the channels are in direct contact with the upper wall. Thus, the flow circulates between channels only. As the aspect ratio decreases, the channel height decreases, and free liquid can also circulate above the channels while circulating in the channels at the same time. As the aspect ratio decreases further, the height of the channels decreases, and the volume of fluid circulating above the channels increases.

4.1. Heat Enhancement Using Nanofluids

A nanofluid composed of 1% vol Al_2O_3 nanoparticles in water is investigated as a working fluid. The flow enters the mixing chamber, then circulates towards the ten mini channels, and exits from the other side of the setup. During its passage, the nanofluid absorbed heat from the bottom of the channel, thus reducing the temperature distribution. The nanoparticle diameter in this particular case is 31 nm.

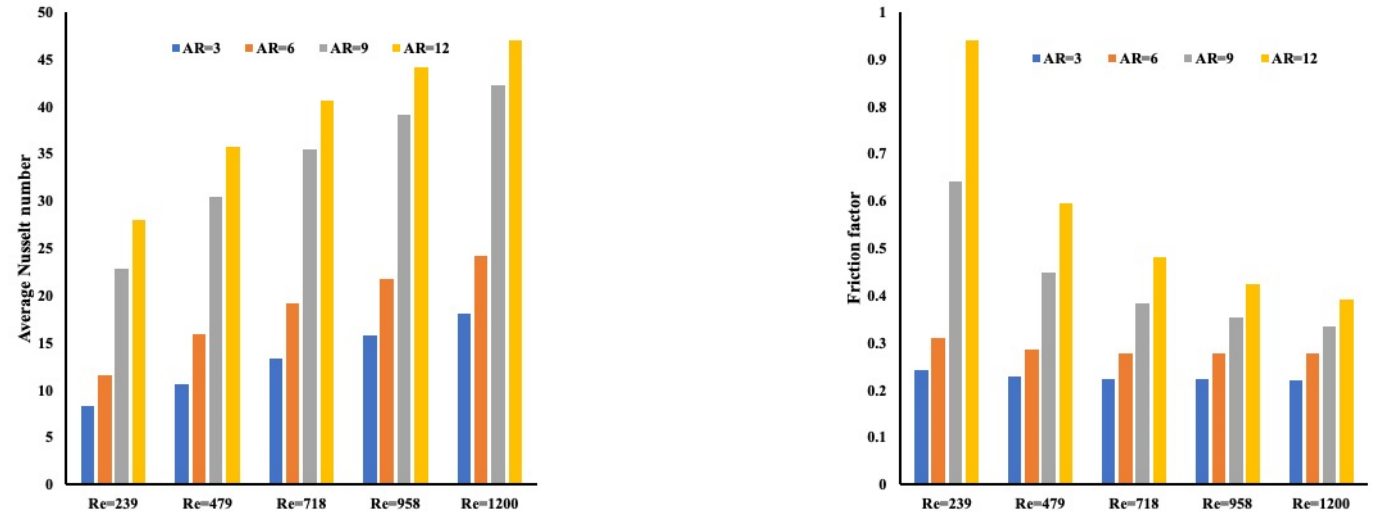
The study is conducted for four different channel heights. It is important to mention that because the volume setup is kept constant for all cases, for an aspect ratio of 3, 6, and 9, the study consists of examining the flow through the channels and circulating in the open space above the channel. When the aspect ratio is set equal to 12, the fluid circulates in the channels only. Five different Reynolds numbers are studied corresponding to different flow rates. Figure 3a presents the temperature distribution along the flow direction 1 mm below the interface, as explained earlier when the aspect ratio is AR = 6. In this particular case, the flow passes through the channel and above the channel at the same time. A reduction in the temperature near the inlet corresponds to large heat extraction by the nanofluid. As the flow circulates, the boundary layer builds up, and the heat enhancement decreases, leading to a higher temperature near the end of the channels. By examining Figure 3b, the local Nusselt number showed a large heat extraction at the beginning and a drastic reduction towards the end of the channels.



(**a**) Temperature variation (**b**) Local Nusselt number

Figure 3. Temperature and local Nusselt number variation for different Reynolds numbers (AR = 6) (dp = 31 nm).

As indicated earlier, the model is solved for all four aspect ratios for all Reynolds numbers. As shown in Figure 4a, a comparison between all cases shows that the average Nusselt number increases as the Reynolds number increases. The highest Nusselt number is found for the aspect ratio of 12, meaning full-height mini channels. In addition, as the aspect ratio increases, the average Nusselt number increases accordingly. The friction factor which relates the fluid entry condition to the pressure drop is shown in Figure 4b. The higher aspect ratio exhibits a high friction factor. This is obvious because the flow is in direct contact with the channel wall; thus, there is a large pressure drop.



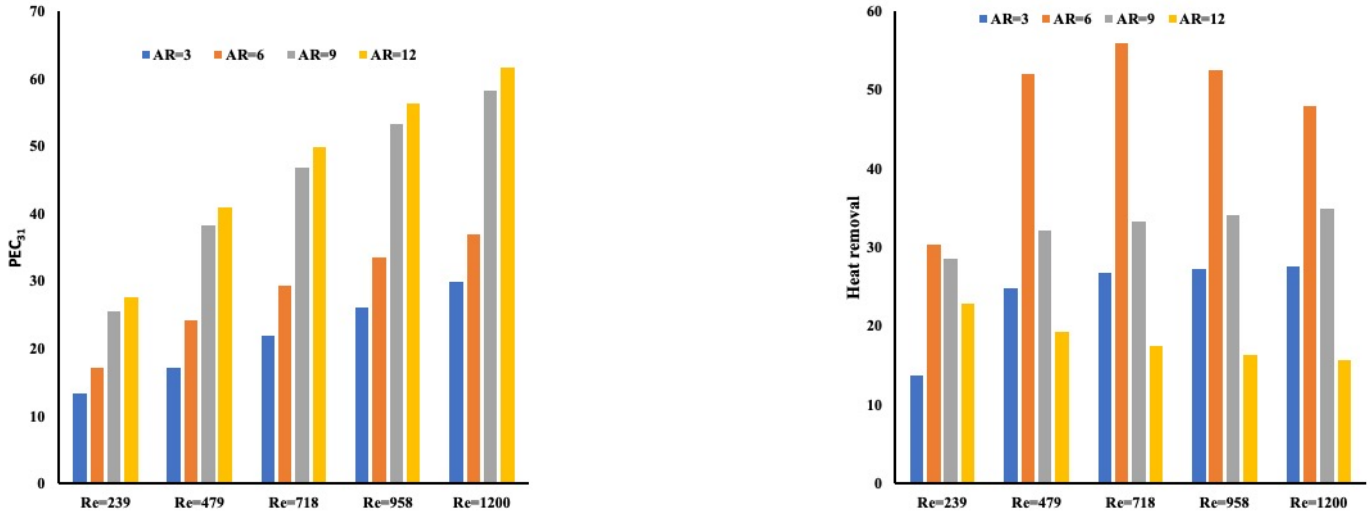
(**a**) Average Nusselt number (**b**) Friction factor for all cases

Figure 4. Average Nusselt number and friction factor for all cases (dp = 31 nm).

However, this friction is noticeable for a low Reynolds number and decreases as the Reynolds number increases, accordingly.

As studied by many researchers, the performance evaluation criterion (PEC) is an important parameter, where one combines the heat effect and the flow effect. The ratio between these two indicator parameters provides a better meaning for the PEC. Figure 5a

provides the performance evaluation criterion for all cases with nanofluids as a circulating fluid using Equation 13. The results revealed that the full height channel provides the best heat performance taking into consideration the flow behavior. This also indicates that for a lower aspect ratio when the flow is moving on top of the channel, no major heat enhancement is observed. If one ignores the pressure drop and studies the optimum design for heat removal, Figure 5b indicates that the best configuration is for an aspect ratio of 6 and a Reynolds number of 718. A previous study by Saghir and Alhajaj [35] using water as a circulating fluid confirmed this finding. It is evident from this observation that flow circulating on top of the channel does have a certain important effect on heat removal. It is interesting to notice that as the Reynolds number increases, the friction decreases, and this is effective for aspect ratios of 9 and 12, respectively. For the lower aspect ratio, no change to the friction factor is observed.



(**a**) Performance evaluation criteria (**b**) Heat removed

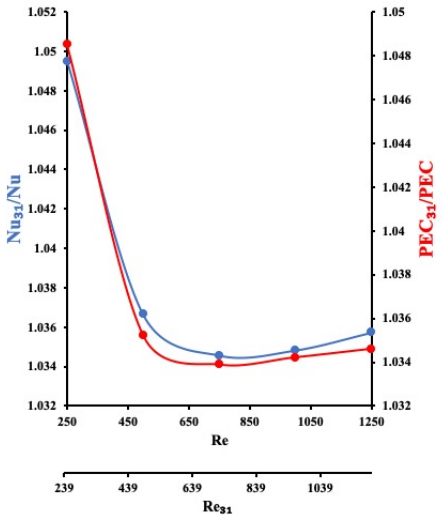
Figure 5. Performance indicator and heat removed for all cases (dp = 31 nm).

4.2. Heat Enhancement Comparison between Water and Nanofluid

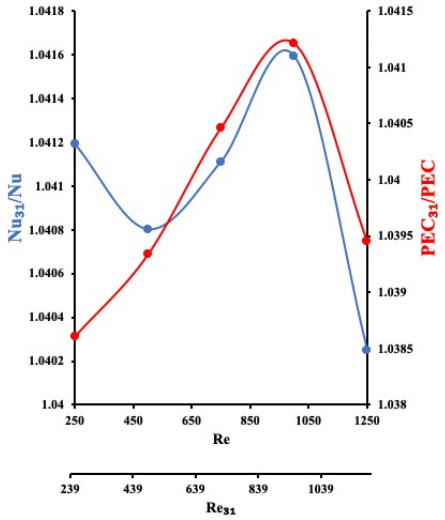
To further investigate the effectiveness of using nanofluid, we have studied the importance of the nanofluid in heat enhancement. A comparison is made between a nanofluid with 31 nm in diameter and water. The presence of nanoparticles increases the conductivity of the fluid when compared to water. Variables with a subscript of 31 or 100 belong to the nanofluid, and the absence of a subscript indicates water.

Figure 6 presents the ratio of the local number between the two cases as well as the performance evaluation criterion for all channels' aspect ratios. As shown in Figure 6a for an aspect ratio of 3, the local Nusselt number variation is similar to both cases; however, the performance of the nanofluid over water varies between 3% and 5%. This shows the usefulness of the nanofluid in heat extraction. An identical observation of the PEC is evident as well in Figure 6a. Here, PEC_{31} means the performance evaluation criterion for a nanofluid with a 31 nm nanoparticle diameter, whereas PEC is the performance evaluation criterion for water. As the aspect ratio increases to 6, Figure 6b shows the two-heat enhancement parameter as a function of Reynolds numbers. The local Nusselt number ratio behaves in a non-linear fashion, and it appears that at a Reynolds number of 1050, one achieves the best performance of heat extraction. A similar trend is observed for the performance evaluation criterion. This behavior is due to the interaction between the flow in the short channel and the flow circulating above the channel. If we continue further in the investigation, as the aspect ratio increases further to 9 and 12, respectively,

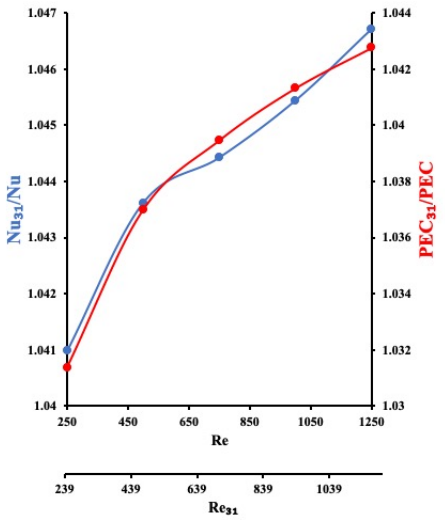
it is evident that the flow is more concentrated in the channel, and thus as the flow rate represented by the Reynolds number increases, the heat extracted represented by the Nusselt number and the performance evaluation criterion increase. An overall observation is that regardless of the aspect ratio, the heat improvement by using the nanofluid does not exceed 5%. Additionally, note that two Reynolds numbers are displayed for each graph. The first one represented by the Reynolds number is for water, and for the identical flow rate, the Re_{31} is for nanofluid. The reason for the difference between the two parameters is the change in the kinematic viscosity for a similar flow rate. It is worth noting that these figures have double axes depending on the fluid used. For an instant, for water circulating in the system, the Reynolds number is 250. For the identical flow rate, the Reynolds number for the nanofluid corresponds to 239.



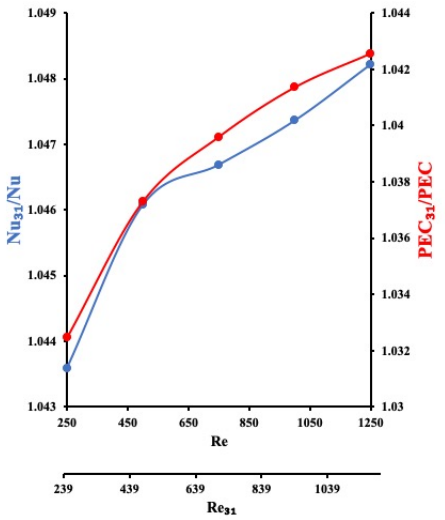
(**a**) Local Nusselt number and performance evaluation criteria (AR = 3)



(**b**) Local Nusselt number and performance evaluation criteria (AR = 6)



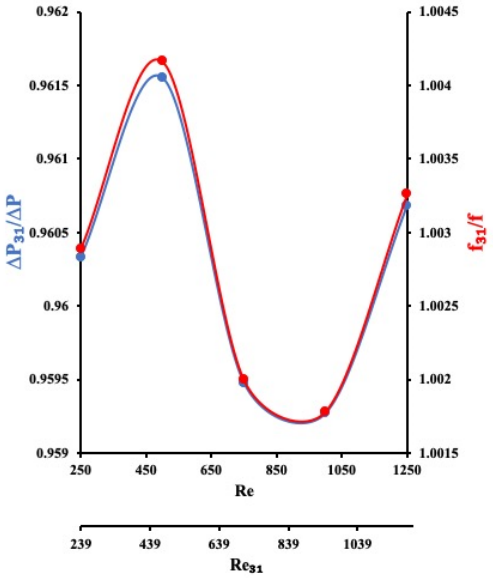
(**c**) Local Nusselt number and performance evaluation criteria (AR = 9)



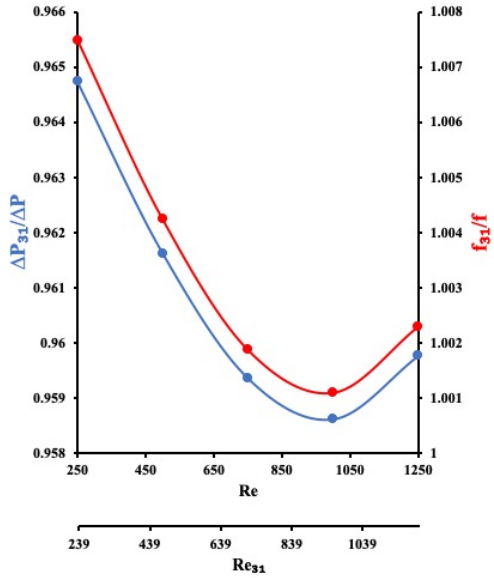
(**d**) Local Nusselt number and performance evaluation criteria (AR = 12)

Figure 6. The ratio of the local Nusselt number and performance criterion between nanofluid and water (dp = 31 nm).

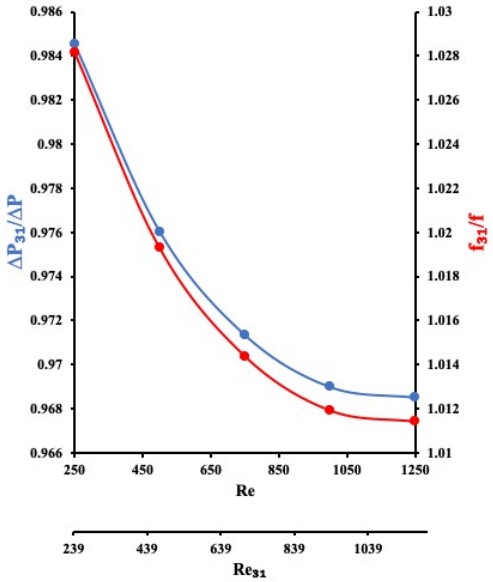
One can also examine two important parameters influencing the performance evaluation criterion, which are the pressure drops and the friction factor. Figure 7 displays these comparisons between water and the nanofluid for the identical flow rate. It is clearly shown that the pressure drop is more pronounced for the nanofluid as the aspect ratio increases in value. It appears that for a lower aspect ratio, allowing the flow to circulate above the channel decreases the pressure drop in the presence of nanofluid when compared to water. However, as the aspect ratio increases, the fluid is confined to the channel leading to a larger pressure drop in the presence of nanofluid. A similar observation is found for the friction factor since both parameters are dependent on each other.



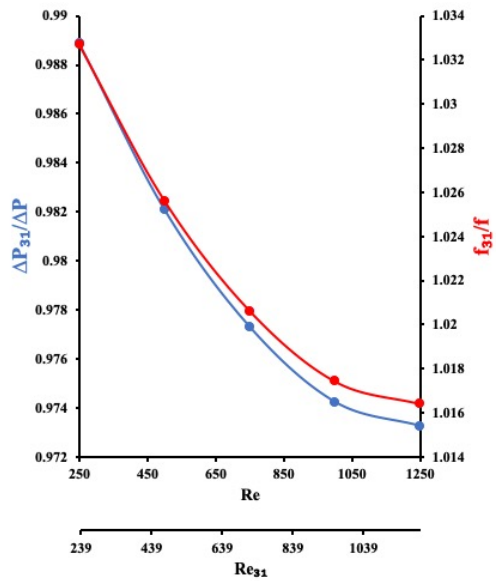
(**a**) Pressure drop and friction factor (AR = 3)



(**b**) Pressure drop and friction factor (AR = 6)



(**c**) Pressure drop and friction factor (AR = 9)



(**d**) Pressure drop and friction factor (AR = 12)

Figure 7. The ratio of the pressure drop and friction factor between nanofluid and water (dp = 31 nm).

4.3. Nanoparticle Size Effect in Heat Removal

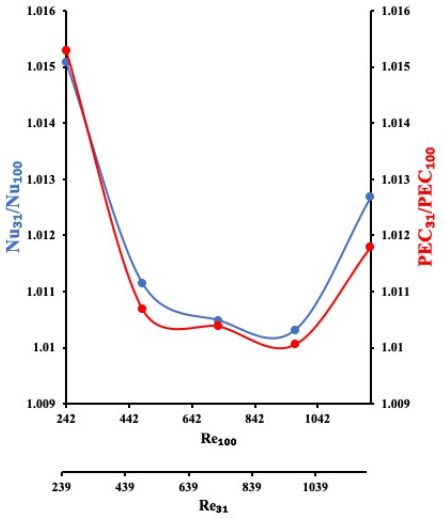
In the previous section, we demonstrated the performance of the nanofluid over water as a working fluid. An enhancement of up to 5% is evident. However, this is at the expense of a larger pressure drop. The performance evaluation criterion combines these two effects of heat removal and friction factor (i.e., pressure drop). The nanoparticle size was 31 nm. In the present study, we investigated the importance of nanoparticle size by comparing the performance of two nanofluids of the same concentration and material but with nanoparticle sizes of 31 nm and 100 nm. Table 1 presents the physical properties of these two nanofluids, and the main difference is the conductivity and the dynamic viscosity. An increase in the thermal conductivity and a decrease in the dynamic viscosity are evident as the number of nanoparticles is less for the same volume percentage. It is important to indicate that a variable with a subscript of 31 (such as Re_{31}, Nu_{31}, PEC_{31}, etc.) belongs to nanofluid having a 31 nm diameter, and there is a similar consideration if the nanoparticles have a 100 nm diameter.

Figure 8 presents the ratios of the Nusselt number and the performance criterion for all aspect ratios. Here, two different Reynolds numbers are shown due to the change of the viscosity of the nanofluid for an identical flow rate. In Figure 8a, one may notice for an aspect ratio of 3 that the heat enhancement is better when the nanoparticle is smaller in size, and this is evident for the performance criterion. The Nusselt number and the PEC number profiles are the same. However, this non-linear behavior is due to the interaction between flow through the short channels and the flow moving above the channel. As the height of the channel changes, Figure 8b presents the case when the aspect ratio is set equal to 6. Non-linear behavior is still evident for the same reason discussed earlier. However, as the aspect ratio increases further, as shown in Figure 8c,d, and as the Reynolds number increases, the Nusselt number and the PEC increase almost linearly because the flow is mostly circulating in the channels. From the overview Figure 8, one may conclude that as the nanoparticle is smaller in size, the heat enhancement, as well as the performance criterion, is better. The improvement is roughly around 2%.

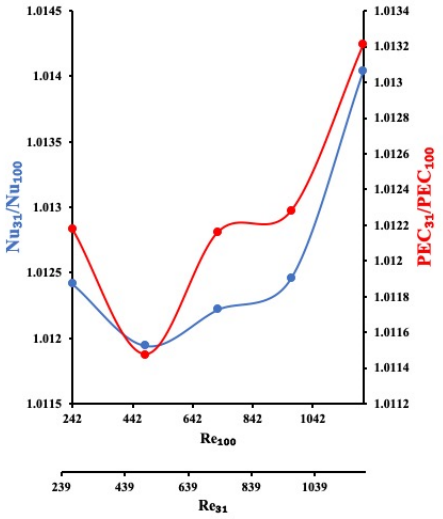
Continuing our investigation, Figure 9 presents the pressure drops and the friction factor for all cases. The reasons for the nanofluid with a 31 nm nanoparticle diameter being better than the 100 nm case is the lower pressure drop and thus the friction factor. In addition, it is noticeable that there is a Reynolds number for which the pressure drop is at its minimum level regardless of the aspect ratio. The Reynolds numbers Re_{31} and Re_{100} near 1000 are determined to be the case.

To investigate the reason behind this matter, the nanoparticles concentrations which are shown in Figures 10 and 11 were examined.

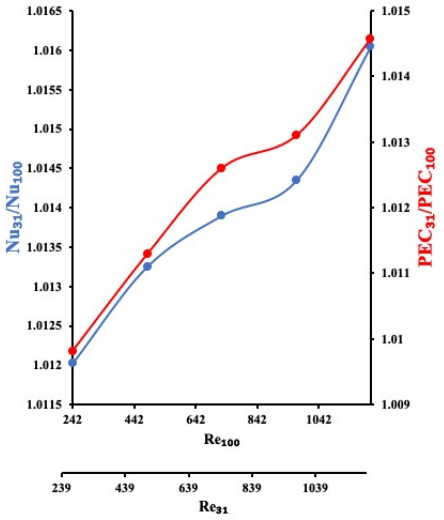
In Figure 10, the concentration is displayed randomly for the case of Re_{31} = 239 and Re_{31} = 1200. For those cases, the size of nanoparticles is 31 nm. Figure 11 presents a similar case when the size of the nanoparticles is 100 nm, corresponding to a Reynolds number Re_{100} = 242 and Re_{100} = 1210. The first observation which is worth noting is that at a lower Reynolds number, as the nanoparticles' size increases, the flow circulating above the channels discourages the nanoparticles from passing through the channel, and thus there are few nanoparticles in the channel. As the Reynolds number increases, for the small nanoparticles case, they pass through the channel due to the interaction between the flow above and in the channels. However, as the nanoparticles increase, fewer nanoparticles in the channels are observed. Additionally, we discover a non-uniform nanoparticle distribution between a channel for one case. This is since the fluid enters around the center of the channel, and thus there is less flow in passing by the channels near the walls of the experimental setup.



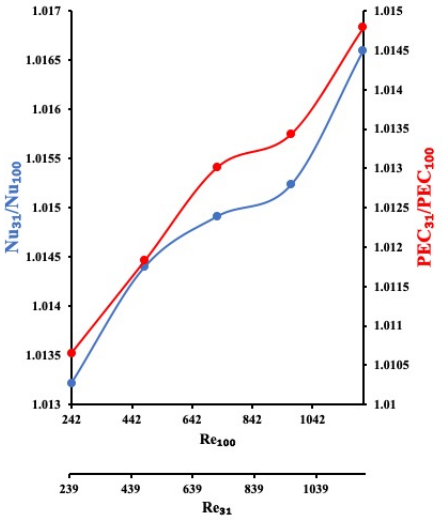
(**a**) Local Nusselt number and performance evaluation criteria (AR = 3)



(**b**) Local Nusselt number and performance evaluation criteria (AR = 6)



(**c**) Local Nusselt number and performance evaluation criteria (AR = 9)



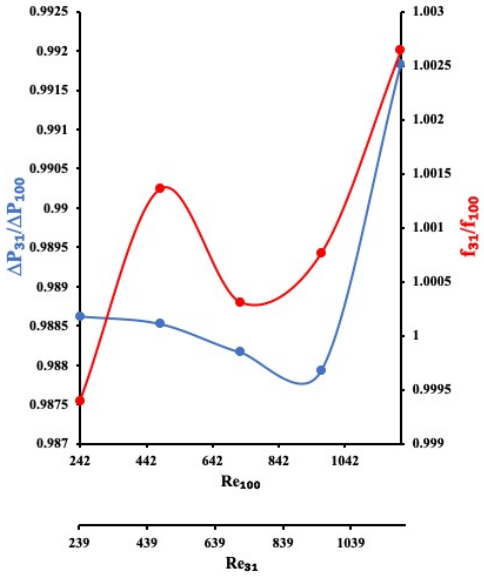
(**d**) Local Nusselt number and performance evaluation criteria (AR = 12)

Figure 8. The ratio of local Nusselt number and performance criterion between nanofluid with different nanoparticles diameter.

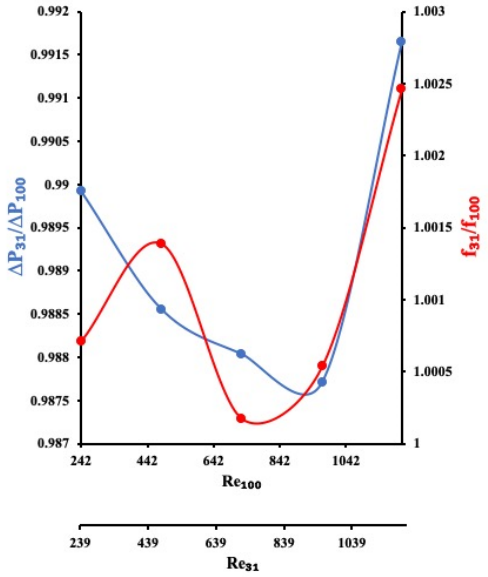
4.4. Heat Performance for All Cases

It is important to assess the performance of different configurations and cases to be able to extrude the best scenario possible for cooling. The novelty of the current work is to investigate the importance of aspect ratio or, in other terms, the channel heights. Additionally, the uniqueness of this study is the flow interaction between the portion circulating inside the channel and passing on top of the channel. This flow behavior is valid only for aspect ratios AR = 3, 6, and 9, respectively. They must be of an optimum configuration that may lead to the best performance of the system.

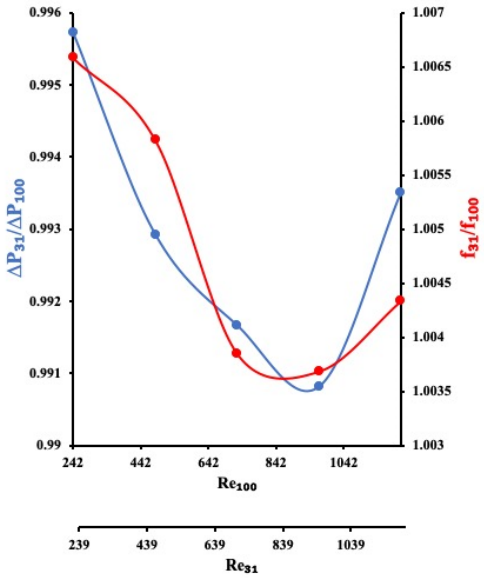
Figure 12 presents the average Nusselt number for all cases of water and nanofluids with a 31 nm nanoparticle diameter and a 100 nm nanoparticle diameter. As observed in Figure 12, as the Reynolds number increases, the Nusselt number increases regardless of the aspect ratio. The change of aspect ratio between 6 and 9 reflects a large average Nusselt slope; then, this slope is reduced as the aspect ratio becomes equal to 12. Then, one may observe a certain optimum aspect ratio leading to the best heat extraction scenario.



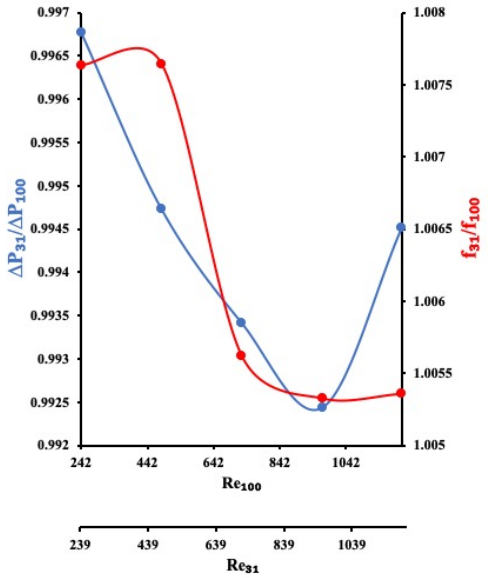
(**a**) Pressure drop and friction factor (AR = 3)



(**b**) Pressure drop and friction factor (AR = 6)



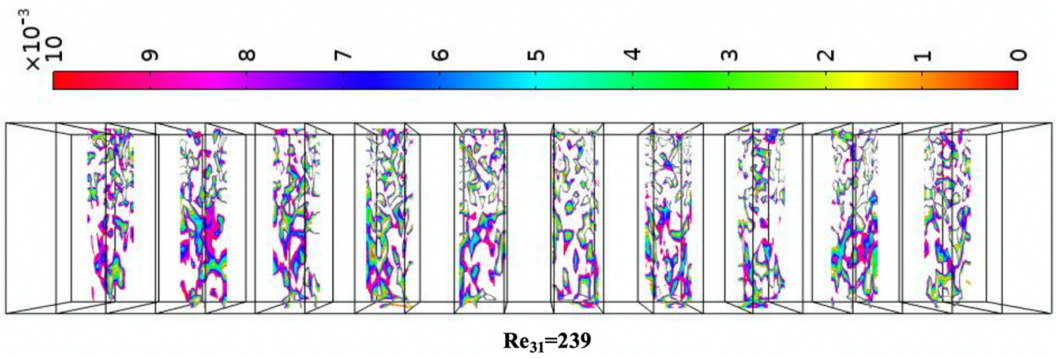
(**c**) Pressure drop and friction factor (AR = 9)



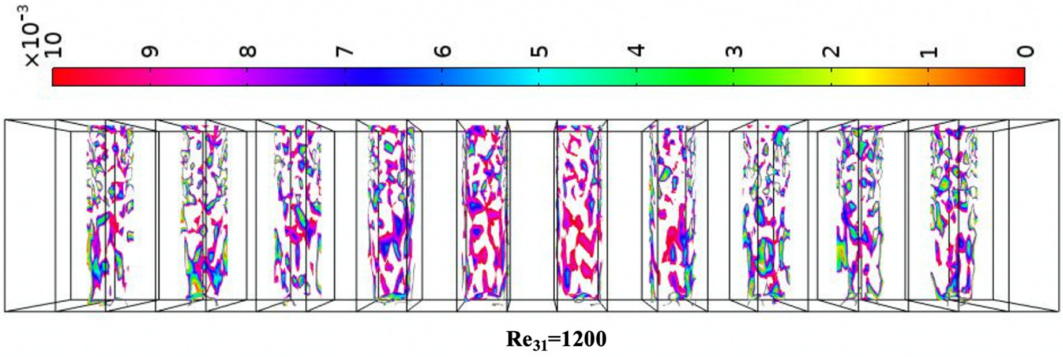
(**d**) Pressure drop and friction factor (AR = 12)

Figure 9. The ratio of the pressure drop and friction factor between nanofluid with different nanoparticles diameter.

Interestingly enough, if one adds the pressure drop or the friction factor, Figure 13 presents the performance criterion. One can see that after an aspect ratio of 9 for the PEC, the slope increase is small; thus, no more improvement is noticeable. Previous results confirmed that for an aspect ratio AR = 12, one has the best PEC. Figure 14 presents the heat removed as a function of the aspect ratio. Here, it contradicts the previous statement and shows that when the aspect ratio is equal to 6, the maximum amount of heat is removed from the system. Thus, if one wishes to ignore the pressure drop effect, adopting an aspect ratio of 6 is the best configuration possible. If the friction needs to be taken into consideration, then an aspect ratio of 12 is the best configuration.

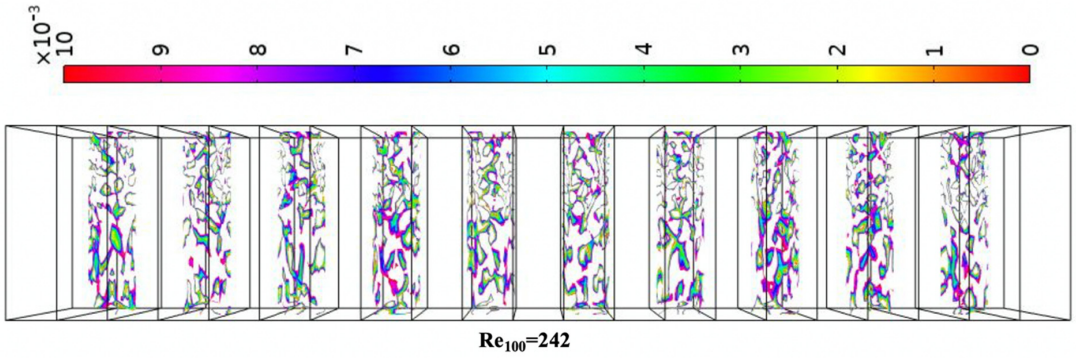


(**a**) Case of Re_{31}=239

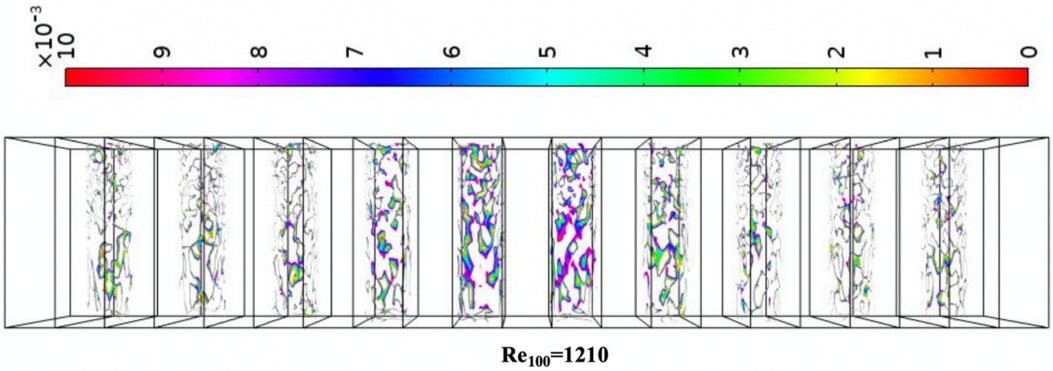


(**b**) case of Re_{31}=1200

Figure 10. Nanoparticles are distributed at the middle of the insert (AR = 6, dp = 31 nm).



(**a**) Case of Re_{100}=242



(**b**) Case of Re_{100}=1210

Figure 11. Nanoparticles are distributed at the middle of the insert (AR = 6, dp = 100 nm).

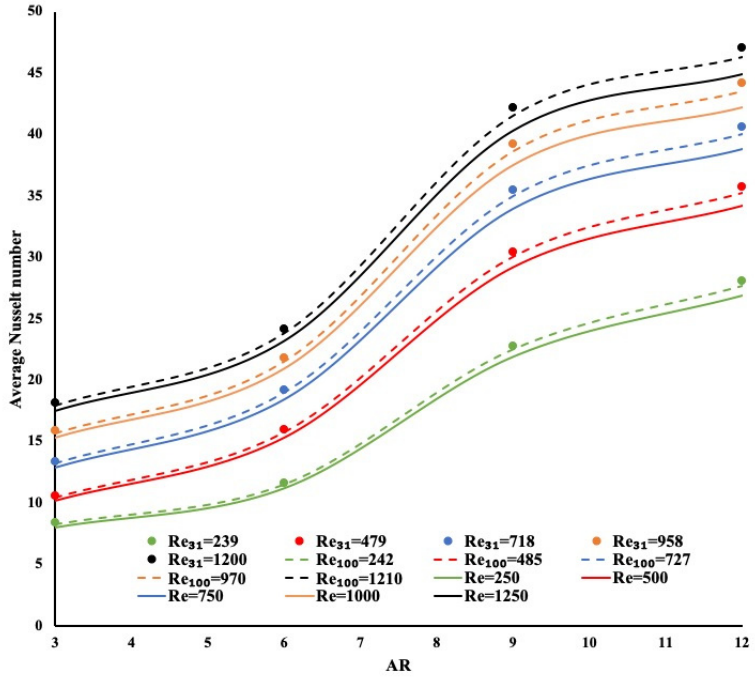


Figure 12. Average Nusselt number for all cases.

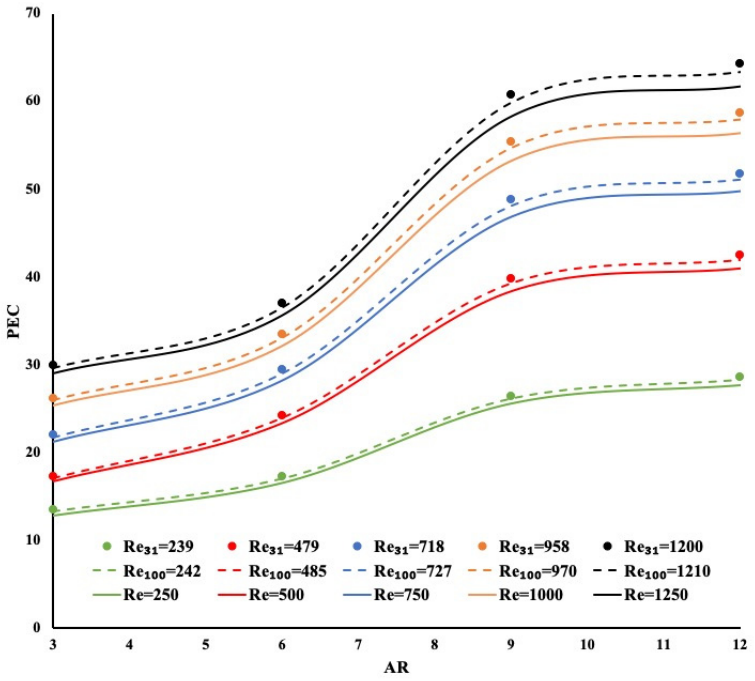


Figure 13. Performance evaluation criteria for all cases.

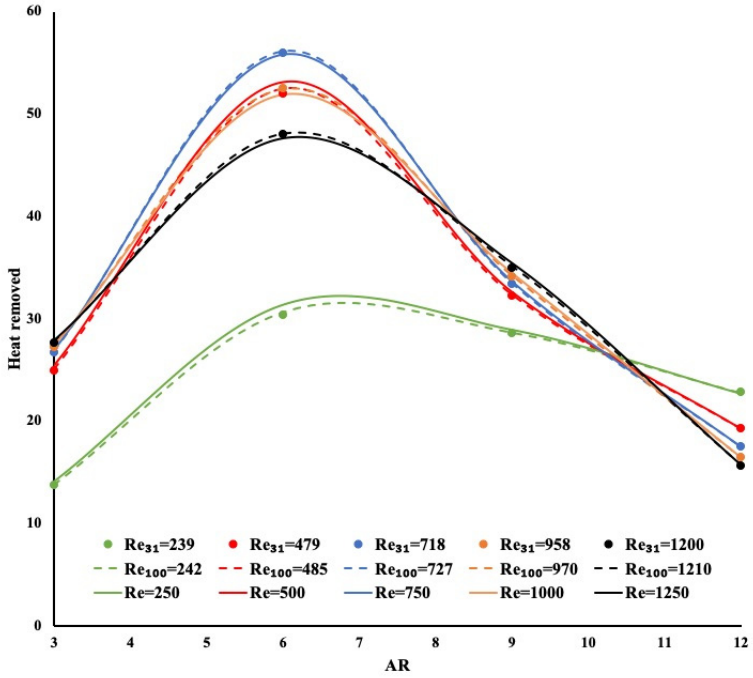


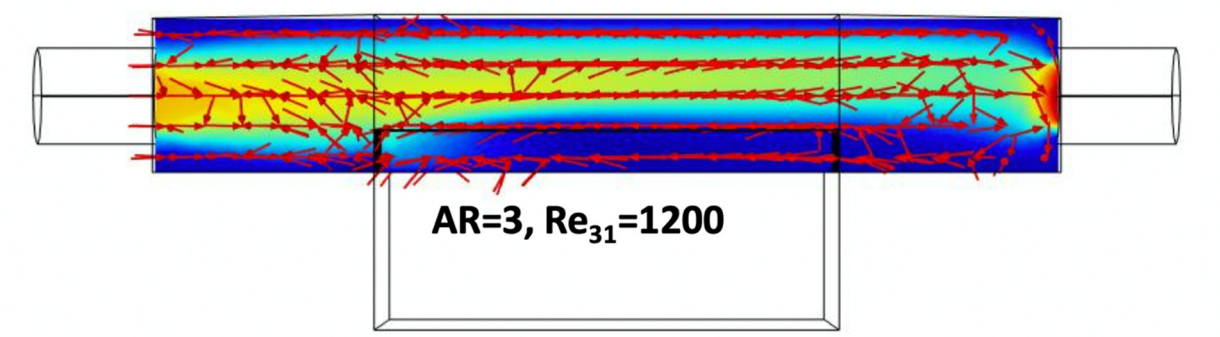
Figure 14. Amount of heat removed for all cases.

4.5. Flow Behavior for Different Aspect Ratio

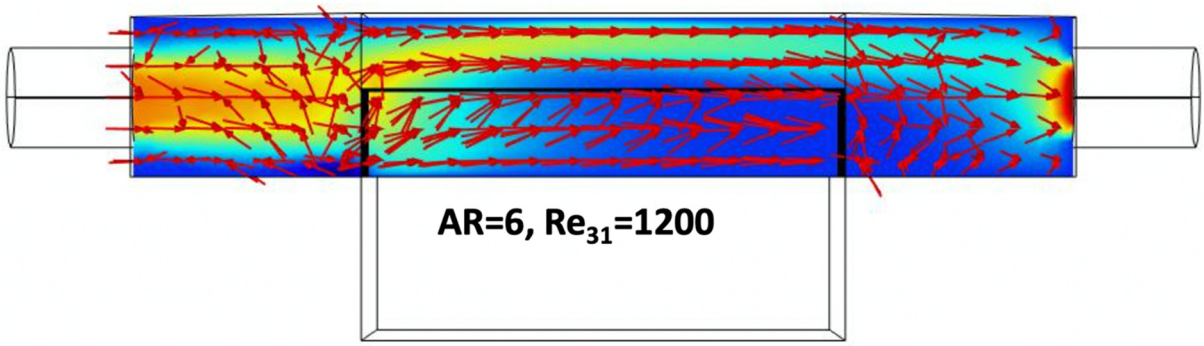
It is interesting to examine the flow behavior which may shed the light on the heat enhancement discussed earlier. Figure 15 presents the flow at the middle of the test section for all aspect ratios and for a Reynolds number Re_{31} set equal to 1200. The nanofluid used in this analysis has a nanoparticle diameter of 31 nm. Four aspect ratios are shown in this figure. By examining Figure 15a, for an aspect ratio AR equal to 3, three backflows are observed. The first one is in the mixing chamber at the entrance. This mixing will not affect the heat removal and has no benefit. The second backflow is observed in the channel. The interaction between the flow passing on the top of the test section and the channel produces a reverse flow. It is for this reason that the temperature on the third part of the channel is low due to major heat enhancement. This means mixing can indeed improve heat removal. The third mixing happens at the exit port of the chamber, which may affect the inlet and outlet pressure.

Figure 15b presents the case when the aspect ratio is 6. This means that half of the test section is covered by the wall of the channels and the other half is a free flow. Besides the two backflows at the inlet and outlet chamber, an interesting flow behavior occurs as it passes through the channels. The flow enters and then moves upward to interact with the free flow passing at the top to descend again and create backflow. It is for this reason that the highest amount of heat removed is found for an aspect ratio AR = 6.

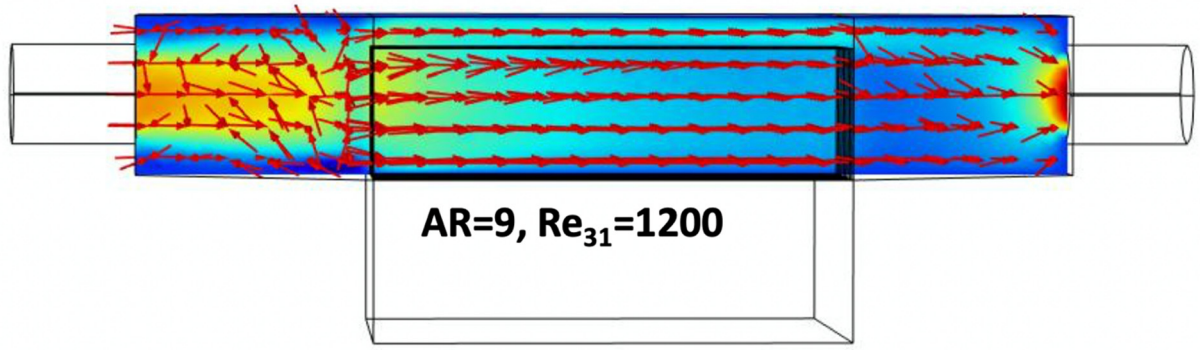
As the aspect ratio increases further, as shown in Figure 15c,d, the flow follows a straight passage through the channel, and heat removal is found to be less than in the previous cases.



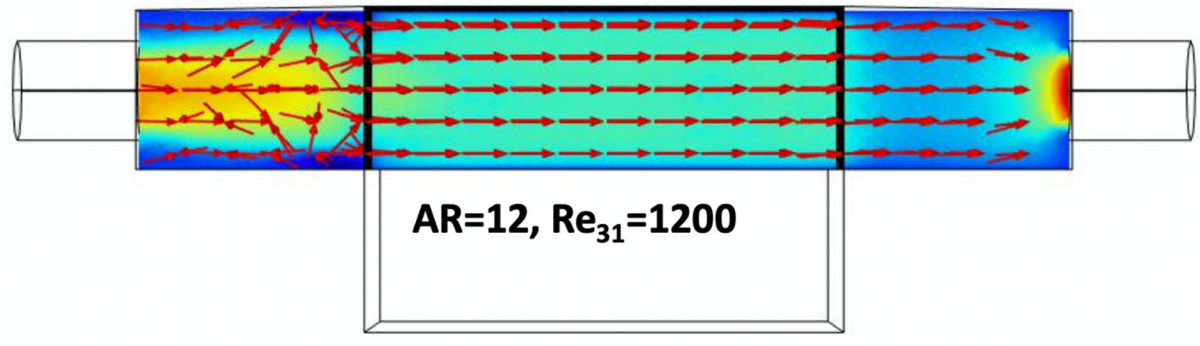
(**a**) Velocity Vectors for AR=3



(**b**) Velocity Vectors for AR=6



(**c**) Velocity Vectors for AR=9



(**d**) Velocity Vectors for AR=12

Figure 15. Flow behavior is at the center of the setup for different aspect ratios.

5. Conclusions

In this paper, attempts are made to investigate the importance of using nanofluid in heat enhancement through mini channels. The uniqueness of this study is varying the channel heights, thus allowing flow to enter the test chamber to circulate inside the mini channel and a portion to circulate on top of the channel. The reason for this interaction taking place is that the total volume of the test section is constant, and as the aspect ratio is below 12, there exists a gap between the channel wall and the test section top wall. This gap allows the flow to circulate in addition to the fluid circulating in the channels. The conclusions from this study are as follows:

1. The reduction of the channel height and the interaction of flow through the channels and passing on top of the channel can reduce the friction factor and therefore the pressure drop.
2. This interaction leads to some backflow, which can enhance the heat removal.
3. If one ignores the pressure drop, a configuration of a channel with an aspect ratio of 6 and flow passing above the channel is the best approach for heat removal.
4. If the pressure drops need to be taken into consideration, it is found that the optimum channel height is 12.
5. For a small aspect ratio of 3 and 6, backflows in three different places are observed and help in heat enhancement at the expense of larger pressure drops.

Author Contributions: Conceptualization, M.Z.S.; methodology, Z.A.H.; software, Z.A.H.; validation, M.Z.S. and Z.A.H.; formal analysis, Z.A.H.; investigation, Z.A.H. and M.Z.S.; resources, M.Z.S.; data curation, Z.A.H.; writing—original draft preparation, M.Z.S. and Z.A.H.; writing—review and editing, Z.A.H.; visualization, Z.A.H. and M.Z.S.; supervision, M.Z.S.; project administration, M.Z.S.; funding acquisition, M.Z.S. All authors have read and agreed to the published version of the manuscript.

Funding: This research was funded by the National Science and Engineering Research Council Canada, Faculty of Engineering and Architecture, Ryerson University; Qatar Foundation, grant number NPRP12S-0123-190011; and the Kuwait Foundation for the Advancement of Sciences (KFAS), project CN20-35EM-04.

Institutional Review Board Statement: Not applicable.

Informed Consent Statement: Not applicable.

Data Availability Statement: Not applicable.

Conflicts of Interest: The authors declare no conflict of interest.

References

1. Saghir, M.Z.; Bayomy, A. Heat enhancement and heat storage for a ternary mixture in a circular pipe. *Therm. Sci. Eng. Prog.* **2018**, *5*, 32–43. [CrossRef]
2. Saghir, M.Z.; Mohamed, A. Effectiveness in incorporating Brownian and thermophoresis effects in modelling convective flow of water-Al_2O_3 nanoparticles. *Int. J. Numer. Methods Heat Fluid Flow* **2018**, *28*, 47–63. [CrossRef]
3. Welsford, C.; Bayomy, A.; Saghir, M. Role of metallic foam in heat storage in the presence of nanofluid and microencapsulated phase change material. *Therm. Sci. Eng. Prog.* **2018**, *7*, 61–69. [CrossRef]
4. Saghir, M.Z.; Bayomy, A.M. Effect of ternary nanoparticles fluid mixture in heat enhancement and heat storage. *Int. J. Aerody.* **2018**, *6*, 85–107. [CrossRef]
5. Saghir, M.Z.; Bayomy, A.M. Experimental measurements and numerical computation of nanofluid and microencapsulated phase change material in porous material. *Int. J. Energy Res.* **2019**, *43*, 6353–6365. [CrossRef]
6. Bayomy, A.; Davies, S.; Saghir, Z. Domestic Hot Water Storage Tank Utilizing Phase Change Materials (PCMs): Numerical Approach. *Energies* **2019**, *12*, 2170. [CrossRef]
7. Bayomy, A.M.; Saghir, Z. Thermal performance of finned aluminum heat sink filled with ERG aluminum foam: Experimental and numerical approach. *Int. J. Energy Res.* **2020**, *44*, 4411–4425. [CrossRef]
8. Alhajaj, Z.; Bayomy, A.; Saghir, M.Z.; Rahman, M. Flow of nanofluid and hybrid fluid in porous channels: Experimental and numerical approach. *Int. J.* **2020**, *1–2*, 100016. [CrossRef]

9. Welsford, C.A.; Delisle, C.S.; Plant, R.D.; Saghir, M.Z. Effects of nanofluid concentration and channeling on the thermal effectiveness of highly porous open-cell foam metals: A numerical and experimental study. *J. Therm. Anal. Calorim.* **2020**, *140*, 1507–1517. [CrossRef]
10. Delisle, C.S.; Welsford, C.A.; Saghir, M.Z. Forced convection study with microporous channels and nanofluid: Experimental and numerical. *J. Therm. Anal. Calorim.* **2019**, *140*, 1205–1214. [CrossRef]
11. Saghir, M.Z.; Welsford, C.; Thanapathy, P.; Bayomy, A.M.; Delisle, C. Experimental Measurements and Numerical Computation of Nano Heat Transfer Enhancement Inside a Porous Material. *J. Therm. Sci. Eng. Appl.* **2020**, *12*, 011003. [CrossRef]
12. Welsford, C.; Thanapathy, P.; Bayomy, A.M.; Ren, M.; Saghir, M.Z. Heat enhancement using aluminum metal foam: Experimental and numerical approach. *J. Porous Media* **2020**, *23*, 249–266. [CrossRef]
13. Plant, R.D.; Hodgson, G.; Impellizzeri, S.; Saghir, M.Z. Experimental and numerical investigation of heat enhancement using a hybrid nanofluid of copper oxide/alumina nanoparticles in water. *J. Therm. Anal. Calorim.* **2020**, *141*, 1951–1968. [CrossRef]
14. Saghir, M.Z.; Rahman, M.M. Forced convection of Al_2O_3–Cu, TiO_2–SiO_2, FWCNT–Fe_3O_4, and ND–Fe_3O_4 hybrid nanofluid in porous media. *Energies* **2020**, *13*, 2902. [CrossRef]
15. Papazian, K.; Al Hajaj, Z.; Saghir, M. Thermal Performance of a Heated Pipe in the Presence of a Metal Foam and Twisted Tape Inserts. *Fluids* **2020**, *5*, 195. [CrossRef]
16. Alhajaj, Z.; Bayomy, A.; Saghir, M. A comparative study on best configuration for heat enhancement using nanofluid. *Int. J.* **2020**, *7–8*, 100041. [CrossRef]
17. Plant, R.D.; Saghir, M.Z. Numerical and experimental investigation of high concentration aqueous alumina nanofluids in a two and three channel heat exchanger. *Int. J.* **2021**, *9*, 100055. [CrossRef]
18. Ho, C.; Liao, J.-C.; Li, C.-H.; Yan, W.-M.; Amani, M. Experimental study of cooling performance of water-based alumina nanofluid in a minichannel heat sink with MEPCM layer embedded in its ceiling. *Int. Commun. Heat Mass Transf.* **2019**, *103*, 1–6. [CrossRef]
19. Ho, C.; Liao, J.-C.; Li, C.-H.; Yan, W.-M.; Amani, M. Experimental study of cooling characteristics of water-based alumina nanofluid in a minichannel heat sink. *Case Stud. Therm. Eng.* **2019**, *14*, 100418. [CrossRef]
20. Hader, M.; Al-Kouz, W. Performance of a hybrid photovoltaic/thermal system utilizing water-Al_2O_3 nanofluid and fins. *Int. J. Energy Res.* **2019**, *43*, 219–230. [CrossRef]
21. Matin, M.H.; Ghanbari, B. Effects of Brownian Motion and Thermophoresis on the Mixed Convection of Nanofluid in a Porous Channel Including Flow Reversal. *Transp. Porous Media* **2014**, *101*, 115–136. [CrossRef]
22. Haddad, Z.; Abu-Nada, E.; Oztop, H.F.; Mataoui, A. Natural convection in nanofluids: Are the thermophoresis and Brownian motion effects significant in nanofluid heat transfer enhancement? *Int. J. Therm. Sci.* **2012**, *57*, 152–162. [CrossRef]
23. Garoosi, F.; Jahanshaloo, L.; Rashidi, M.M.; Badakhsh, A.; Ali, M. Numerical simulation of natural convection of the nanofluid in heat exchangers using a Buongiorno model. *Appl. Math. Comput.* **2015**, *254*, 183–203. [CrossRef]
24. Malvandi, A.; Moshizi, S.A.; Soltani, E.G.; Ganji, D.D.G.-D. Modified Buongiorno's model for fully developed mixed convection flow of nanofluids in a vertical annular pipe. *Comput. Fluids* **2014**, *89*, 124–132. [CrossRef]
25. Yazdi, M.E.; Nejad, A.K.; Dinarvand, S.; Tamim, H. Brownian Motion Effects on Natural Convection of Alumina-Water Nanofluid in 2-D Enclosure. *Heat Transf.-Asian Res.* **2014**, *43*, 720–733. [CrossRef]
26. Prasher, R.; Bhattacharya, P.; Phelan, P. Brownian-Motion-Based Convective-Conductive Model for the Effective Thermal Conductivity of Nanofluids. *J. Heat Transf.* **2005**, *128*, 588–595. [CrossRef]
27. Durgaprasad, P.; Varma, S.V.K.; Hoque, M.M.; Raju, C.S.K. Combined effects of Brownian motion and thermophoresis parameters on three-dimensional (3D) Casson nanofluid flow across the porous layers slendering sheet in a suspension of graphene nanoparticles. *Neural Comput. Appl.* **2018**, *31*, 6275–6286. [CrossRef]
28. Rafique, K.; Anwar, M.I.; Misiran, M.; Khan, I.; Seikh, A.H.; Sherif, E.-S.M.; Nisar, K.S. Brownian Motion and Thermophoretic Diffusion Effects on Micropolar Type Nanofluid Flow with Soret and Dufour Impacts over an Inclined Sheet: Keller-Box Simulations. *Energies* **2019**, *12*, 4191. [CrossRef]
29. Lin, Y.; Jiang, Y. Effects of Brownian motion and thermophoresis on nanofluids in a rotating circular groove: A numerical simulation. *Int. J. Heat Mass Transf.* **2018**, *123*, 569–582. [CrossRef]
30. Bondareva, N.S.; Sheremet, M.A.; Öztop, H.F.; Abu-Hamdeh, N. Transient natural convection in a partially open trapezoidal cavity filled with a water-based nanofluid under the effects of Brownian diffusion and thermophoresis. *Int. J. Numer. Methods Heat Fluid Flow* **2018**, *28*, 606–623. [CrossRef]
31. Sheremet, M.A.; Pop, I. Free convection in a triangular cavity filled with a porous medium saturated by a nanofluid: Buongiorno's mathematical model. *Int. J. Numer. Methods Heat Fluid Flow* **2015**, *25*, 1138–1161. [CrossRef]
32. Khan, J.A.; Mustafa, M.; Hayat, T.; Turkyilmazoglu, M.; Alsaedi, A. Numerical study of nanofluid flow and heat transfer over a rotating disk using Buongiorno's model. *Int. J. Numer. Methods Heat Fluid Flow* **2017**, *27*, 221–234. [CrossRef]
33. Saghir, M.; Rahman, M. Brownian motion and thermophoretic effects of flow in channels using nanofluid: A two-phase model. *Int. J.* **2021**, *10*, 100085. [CrossRef]
34. Saghir, M.; Rahman, M. Forced convection in multichannel configuration in the presence of blocks insert along the flow path. *Int. J.* **2021**, *10*, 100089. [CrossRef]
35. Saghir, M.Z.; Alhajaj, Z. Optimum Multi-Mini-Channels Height for Heat Enhancement under Forced Convection Condition. *Energies* **2021**, *14*, 7020. [CrossRef]